

FROM MICRO TO MACRO DYNAMICS VIA A NEW CLOSURE APPROXIMATION TO THE FENE MODEL OF POLYMERIC FLUIDS*

PENG YU[†], QIANG DU[†], AND CHUN LIU[†]

Abstract. We present a new closure approximation needed for deriving effective macroscopic moment equations from the microscopic finite-extensible-nonlinear-elastic kinetic theory modeling viscoelastic polymeric fluids. The closure is based on restricting the otherwise general probability distribution functions (PDFs) to a class of smooth distributions motivated by perturbing the equilibrium PDF. The simplified system coupling the moment equations and the Navier–Stokes equations still possesses an energy law analogous to the original micro-macro system. Some theoretical analysis and numerical experiments are presented to ensure the validity of the moment-closure system, and to illustrate the excellent agreement of the simplified model with the original system solved using a Monte Carlo approach, for a certain regime of physical parameters.

Key words. multiscale modeling, micro-macro dynamics, polymeric fluid, non-Newtonian fluid, finite-extensible-nonlinear-elastic model, moment closure, existence of solution, Monte Carlo, Fokker–Planck, numerical simulation

AMS subject classifications. 76A05, 76M99, 65C30

DOI. 10.1137/030602794

1. Introduction. There are two major approaches to the modeling of non-Newtonian polymeric fluids: the continuum (or macroscopic) approach and the multiscale (or micro-macro) approach. In the continuum approach (see, e.g., [1, 29]), either algebraic or differential macroscopic constitutive equations are introduced to account for the distinct non-Newtonian features of the stress induced by the macromolecules, such as shear-rate dependent viscosity, viscoelastic memory effect, etc. On the other hand, the multiscale approach (see, e.g., [2, 7]) couples the macroscopic description of the fluid flow with consideration of the detailed polymer structure, such as the stretching and the orientation of the polymer molecules. Although the micro-macro approach provides more detailed information on the microstructure of the polymeric fluids, it is also much more demanding computationally than the purely macroscopic approach. It is thus desirable and sometimes necessary to somehow reduce a microscopic or micro-macro model to one that is defined completely by macroscopic quantities while still capturing the essential influences on the bulk flow phenomena. Unfortunately, this *coarse-graining* can be done without resorting to approximations only for the crudest kinetic theory on Hookean dumbbells. In this paper, we present a new moment-closure approximation that enables us to derive, for a certain regime of physical parameters, effective macroscopic equations for the finite-extensible-nonlinear-elastic (FENE) dumbbell model [2].

A general micro-macro elastic dumbbell model for dilute polymer solutions can be written as a coupled system of the incompressible Navier–Stokes equations describing the macroscopic flow field $\vec{u} = \vec{u}(\vec{x}, t)$ and a Fokker–Planck equation describing the probability distribution function (PDF) $f = f(\vec{x}, \vec{Q}, t)$ on the molecular level of the

*Received by the editors December 31, 2003; accepted for publication (in revised form) April 30, 2004; published electronically March 25, 2005. This research was supported in part by NSF grants DMS-0196522 and ITR-0205232.

<http://www.siam.org/journals/mms/3-4/60279.html>

[†]Department of Mathematics, Pennsylvania State University, University Park, PA 16802 (pyu@math.psu.edu, qdu@math.psu.edu, liu@math.psu.edu).

dumbbell orientation \vec{Q} [2, 28],

$$(1.1) \quad \frac{\partial \vec{u}}{\partial t} + (\vec{u} \cdot \nabla) \vec{u} + \nabla p = \nabla \cdot \tau_p + \nu \Delta \vec{u},$$

$$(1.2) \quad \nabla \cdot \vec{u} = 0,$$

$$(1.3) \quad \frac{\partial f}{\partial t} + (\vec{u} \cdot \nabla) f + \nabla_{\vec{Q}} \cdot (\nabla \vec{u} \vec{Q} f) = \frac{2}{\zeta} \nabla_{\vec{Q}} \cdot (\nabla_{\vec{Q}} \Psi f) + \frac{2\mathcal{K}\mathcal{T}}{\zeta} \Delta_{\vec{Q}} f.$$

In the Navier–Stokes equation (1.1), p is the hydrostatic pressure, ν is the fluid viscosity, and τ_p is a tensor representing the polymer contribution to stress,

$$(1.4) \quad \tau_p = \lambda \int (\nabla_{\vec{Q}} \Psi \otimes \vec{Q}) f(\vec{x}, \vec{Q}, t) d\vec{Q},$$

where $\Psi(\vec{Q})$ is the elastic spring potential to be specified later, and λ is the polymer density constant. In the Fokker–Planck equation (1.3), ζ is the friction coefficient of the dumbbell beads, \mathcal{T} is the temperature, and \mathcal{K} is the Boltzmann constant. Equation (1.2) is the usual incompressibility condition.

The simplest spring potential is given by the Hookean law $\Psi(\vec{Q}) = HQ^2/2$, where $Q = |\vec{Q}|$ and H is the elasticity constant. In fact, exploiting this simple potential, one can derive a macroscopic differential constitutive equation for the polymeric stress τ_p from the Fokker–Planck equation, which leads to the so-called Oldroyd-B fluids. However, for a more practical FENE potential that takes into account a finite-extensibility constraint, $\Psi(\vec{Q}) = -(HQ_0^2/2) \log(1 - (Q/Q_0)^2)$, there does not exist an exact macroscopic constitutive equation for τ_p , and certain approximations need to be introduced. Here Q_0 is the maximum dumbbell extension. The FENE spring force law reads

$$(1.5) \quad \nabla_{\vec{Q}} \Psi = \frac{H\vec{Q}}{1 - (Q/Q_0)^2}.$$

For convenience of later discussions, we state the equilibrium PDF corresponding to the FENE potential, i.e., the equilibrium solution to the Fokker–Planck equation under zero flow field,

$$(1.6) \quad f_{\text{eq}} = \frac{1}{J_{\text{eq}}} e^{-\Psi/\mathcal{K}\mathcal{T}} = \frac{1}{J_{\text{eq}}} \left[1 - \left(\frac{Q}{Q_0} \right)^2 \right]^{HQ_0^2/2\mathcal{K}\mathcal{T}},$$

where J_{eq} is a normalizing factor.

Simulating the coupled micro-macro system numerically is a demanding task, in that at each spatial point \vec{x} the configuration space of \vec{Q} needs to be resolved or at least sampled. Recently, Lozinski and Chauviere [25] have introduced a fast solver to tackle the Fokker–Planck equation directly with a novel time splitting scheme. However, a more widely used method to solve the coupled system is the so-called CONFFESSIT approach [22] that simulates the stochastic differential equation corresponding to the Fokker–Planck equation to achieve a Monte Carlo sampling of the configuration space. The latter approach has the advantage that the complexity increases only mildly as the model extends to include multibead polymer chains. Since the statistical error decays very slowly in the total number of sample Brownian particles, a major issue is how to reduce the statistical error bars while still preserving the mean values of the quantities of interest. To this end, various variance reduction

techniques based on control variate [3, 26] and importance sampling [26] have been introduced. The Brownian configuration field (BCF) method [17], which is widely accepted as an efficient variant of the original CONNFESSIT approach, can also be regarded as a variance reduction technique [27], in which the neighboring grid points serve as control variates for each other. The well-posedness of the BCF formulation, the convergence of the numerical methods based on the BCF, and the specific patterns in which the BCF achieves variance reduction have been studied extensively by Jourdain, Lelievre, and Le Bris [18, 19, 20]. However, the Monte Carlo approach is still very expensive, even in its most efficient BCF form.

If we call the above approaches based on Monte Carlo sampling or the Fokker–Planck equation the detailed simulation methods, an attractive alternative, which we pursue in this paper, is to derive simplified models from the Fokker–Planck equation with closure approximations valid for a certain regime of physical parameters. The advantage of this approach is that the resulting simplified model consists only of macroscopic quantities, and the dependence on the configuration space will be integrated out, which drastically reduces the computational cost. In a typical derivation of the moment-closure equations, one multiplies the Fokker–Planck equation by certain powers of \bar{Q} and integrates over the configuration space. Upon integration by parts, most of the terms in the coarse-grained equations can be expressed in terms of the selected moments, except for those involving $\nabla\Psi$, which need to be related to the selected moments by certain closure approximations. Such approximations are usually inspired by the equilibrium distributions. For example, it is well known that, in the Gaussian case, the higher moments can be determined by the first two moments via the Wick’s theorem [26].

Motivated by the observation that each moment-closure relation implicitly defines a subclass of the underlying PDFs, we start by first introducing a novel class of smooth distribution functions to which we restrict the solutions of the Fokker–Planck equation. The class of PDFs that we choose can be viewed as a perturbation to the equilibrium PDF (1.6) and is parameterized by three variables which have a simple correspondence with the second moments of the PDF. This restricted class still allows for the existence of normal stress difference and shear stress, which are closely related to many distinct features of non-Newtonian fluids [1]. Moreover, the proposed class of PDFs possesses a simple structure so that all integrations in the derivation of the moment-closure equations can be performed analytically without making further approximations. Hence, we are able to explicitly write down the resulting moment-closure system, which is a set of macroscopic PDEs involving only the independent variables \vec{x} and t , in place of the original Fokker–Planck equation, which is defined on both the physical and configuration spaces.

Owing to the simple form of the resulting system, we are able to show that the new coupled system of the Navier–Stokes equation and the moment equations satisfies an energy law analogous to the one for the original FENE model. The local well-posedness of the new system can also be established. In order to validate the simplified model against the detailed simulation method, we perform numerical simulations using the new moment-closure system and the BCF method on two types of flow problems: simple shear flow and driven-cavity flow (and some variants). In the former case, we solve the moment equations alone (decoupled from the flow calculation) and compare the stress predicted by this simplified model with that obtained by solving the Fokker–Planck equation directly. We find that the agreement of the predicted stresses is very good for relatively small shear rates, even though the probability distributions obtained by the two methods differ significantly. This manifests nicely the philosophy

behind the moment-closure approach. Namely, *the important degrees of freedom are captured, although the fully detailed distribution space is not completely resolved*. For the latter case of driven-cavity flow, we solve the coupled system of the Navier–Stokes equation and the moment equations and compare in detail the flow and stress fields with those obtained from Monte Carlo simulation. For a certain regime of physical parameters, we find that the agreement of the moment-closure results and the averaged Monte Carlo results is excellent. Furthermore, we will reinforce the important role played by our ansatz on the restricted class of probability distributions by showing that ignoring certain terms in the ansatz leads to dramatically different flow patterns than in Monte Carlo simulation.

There are many other existing closure approximations to the FENE model, for example the FENE-P model [1] and the FENE-L model [23, 24]. Although the original derivation of the FENE-P model is based on an ad hoc averaging assumption, it can also be derived by a similar strategy as described above, provided that the restricted class of PDFs is taken as symmetric Dirac distributions, as shown in [23, 24]. Meanwhile, Lielens et al. [23] and Lielens, Keunings, and Legat [24] also point out that, since the restricted class associated with the FENE-P model is a one-parameter family, the hysteretic behavior of FENE fluids cannot be recovered by the FENE-P model. Consequently, the same authors have proposed a new closure model named FENE-L, which is derived by restricting the PDFs to a class defined by L-shaped distributions assembled from Heaviside and Dirac delta functions. The FENE-L model has the obvious advantage of being able to capture PDFs far away from equilibrium, and it has been shown to be able to qualitatively recover the hysteretic behavior of the original FENE fluids. However, no results have been shown for coupling the calculation of the flow field by the Navier–Stokes equation with the simplified FENE-L model. The major difference in our approach is that the class of PDFs to be proposed later consists of *smooth* distribution functions motivated by perturbing the equilibrium distribution (1.6). Moreover, we may establish an energy law for our simplified model that is similar to the one for the original FENE model. More detailed comparisons of our model with the FENE-L model, especially in terms of their time-dependent behaviors, are currently under investigation.

It is also illuminating to sketch similar works on a different micro-macro model, the Doi model of liquid-crystalline polymers [7]. The Doi model is based on modeling polymer molecules as rigid axisymmetric rods of infinite aspect ratio, and the theory provides a Fokker–Planck equation for the distribution for the orientation distribution function defined on the surface of a unit sphere. There exist a variety of ad hoc closure approximations to the Doi-type kinetic theory [7, 16], which have been systematically compared for simple elongational and fiber flows by Wang [31, 32] and for shear flows by Forest, Wang, and Zhou [13]. On the other hand, following the work of Feng, Chaubal, and Leal [11] and Feng and Leal [12] on complex flows in eccentric cylinder geometry, Grosso et al. [15] have illustrated the insufficiency of the ad hoc quadratic closure to capture many qualitative aspects of the exact solution. This brings out the importance of following the more systematic approach of restricting to a prescribed class of PDFs. For the Doi model, the Bingham distribution provides a natural candidate, which can be shown to contain the exact steady-state solutions of the Doi model for homogeneous irrotational flow or purely rotational flow [4]. It is shown in [15] that, with the Bingham closure, a qualitative agreement with the exact solution can be obtained, at least for slow flows. However, a major issue with the Bingham closure is that the moments of the Bingham distribution cannot be evaluated analytically, and thus the resulting system cannot be expressed in a simple

form. Rather involved numerical procedures have to be introduced to complete the implementation of the closure equations [4, 14].

We now give an outline of this paper. The new moment-closure procedure is described in section 2. The mathematical analysis on the local well-posedness of the resulting system is briefly discussed in section 3. Extensive comparison of the simulation results using new moment-closure model and the detailed simulation methods is given in section 4 on two types of flow problems: simple shear flow and driven-cavity flow. Numerical results on some variants of the driven-cavity flow using other boundary conditions are also presented. A summary and an outlook for future work are given at the end.

2. A new closure approximation. For simplicity of the presentation, we formulate our moment-closure in two dimensions. Generalization to the three-dimensional case is readily available. Motivated by the observation that each moment-closure relation implicitly defines a subclass of the underlying PDFs, we start by first introducing a class of PDFs which gives rise to a systematic way to derive closure approximations,

$$(2.1) \quad f(\vec{Q}) = \frac{1}{J_b} \left[1 - \left(\frac{Q}{Q_0} \right)^2 \right]^{b/2} (1 + \beta Q_1 Q_2 + \gamma(Q_1^2 - Q_2^2)),$$

where $\vec{Q} = (Q_1, Q_2)$, and J_b is scaling constant such that $\int f(\vec{Q})d\vec{Q} = 1$. When the three parameters b , β , and γ take the values HQ_0^2/KT , 0, and 0, respectively, the distribution (2.1) reduces to the equilibrium distribution (1.6). Hence, one may view (2.1) as a perturbation to the equilibrium distribution. Notice that (2.1) is symmetric under the transformation $\vec{Q} \rightarrow -\vec{Q}$, which reflects the fact that the two beads of the dumbbell are treated identically in the FENE model.

Owing to the simple structure of (2.1), one may derive, without any further approximation, simple correspondences between the parameters b , β , and γ and the second order moments $\langle Q_1^2 \rangle$, $\langle Q_2^2 \rangle$, and $\langle Q_1 Q_2 \rangle$ of the PDF, where brackets denote averaging with respect to the PDF (2.1). The following formula proves very useful in the computation [2]:

$$(2.2) \quad \int_0^{R_0} \left[1 - \left(\frac{R}{R_0} \right)^2 \right]^b R^n dR = \frac{1}{2} R_0^{n+1} B \left(\frac{n+1}{2}, \frac{b+2}{2} \right),$$

where $B(x, y) = \Gamma(x)\Gamma(y)/\Gamma(x+y)$ and $\Gamma(x)$ is the gamma function. Exploiting the special symmetry of (2.1) and using (2.2) repetitively, one can easily check that

$$(2.3) \quad \langle Q^2 \rangle = \langle Q_1^2 + Q_2^2 \rangle = \frac{2Q_0^2}{b+4},$$

$$(2.4) \quad \langle Q_1^2 - Q_2^2 \rangle = \frac{4\gamma Q_0^4}{(b+4)(b+6)},$$

$$(2.5) \quad \langle Q_1 Q_2 \rangle = \frac{\beta Q_0^4}{(b+4)(b+6)}.$$

Or solving for b , β , and γ , we obtain

$$(2.6) \quad b = \frac{2Q_0^2}{\langle Q^2 \rangle} - 4,$$

$$(2.7) \quad \beta = \frac{\langle Q_1 Q_2 \rangle (b+4)(b+6)}{Q_0^4} = 4 \langle Q_1 Q_2 \rangle \left(\frac{1 + \langle Q^2 \rangle / Q_0^2}{\langle Q^2 \rangle^2} \right),$$

$$(2.8) \quad \gamma = \frac{\langle Q_1^2 - Q_2^2 \rangle (b+4)(b+6)}{4Q_0^4} = \langle Q_1^2 - Q_2^2 \rangle \left(\frac{1 + \langle Q^2 \rangle / Q_0^2}{\langle Q^2 \rangle^2} \right).$$

Hence, the parameter b can be easily determined from the variance $\langle Q^2 \rangle$ of the PDF, and β and γ depend linearly on $\langle Q_1 Q_2 \rangle$ and $\langle Q_1^2 - Q_2^2 \rangle$ up to a factor depending on b . This rather transparent correspondence allows us to arrive at simple moment-closure equations on which mathematical analysis is feasible.

Now we are ready to derive the moment equations from the Fokker–Planck equation (1.3). We first consider the moment $\langle Q^2 \rangle = \langle Q_1^2 + Q_2^2 \rangle$. Multiplying (1.3) by $Q_1^2 + Q_2^2$ and integrating by parts, one gets

$$(2.9) \quad \begin{aligned} \frac{\partial}{\partial t} \langle Q^2 \rangle + \vec{u} \cdot \nabla \langle Q^2 \rangle - 2 \left(\frac{\partial u}{\partial y} + \frac{\partial v}{\partial x} \right) \langle Q_1 Q_2 \rangle \\ - \left(\frac{\partial u}{\partial x} - \frac{\partial v}{\partial y} \right) \langle Q_1^2 - Q_2^2 \rangle = \frac{8\mathcal{K}\mathcal{T}}{\zeta} - \frac{4}{\zeta} \int (\nabla_{\vec{Q}} \Psi \cdot \vec{Q}) f d\vec{Q}. \end{aligned}$$

In general, the term $\int (\nabla_{\vec{Q}} \Psi \cdot \vec{Q}) f d\vec{Q}$ cannot be expressed by the second moments, and thus certain closure assumptions have to be made to relate this term to the selected moments approximately. This can be achieved by resorting to the ansatz (2.1). More specifically, we assume that the solution to the Fokker–Planck equation takes the specific form in (2.1) which leads to the expression

$$(2.10) \quad \int (\nabla_{\vec{Q}} \Psi \cdot \vec{Q}) f d\vec{Q} = \frac{2HQ_0^2}{b}.$$

This closure procedure is equivalent to requesting that the trajectory of the moments dictated by the simplified moment equations stays tangential to the trajectory of the moments by solving Fokker–Planck equation directly, provided that the solution to the Fokker–Planck equation belongs to the class (2.1) at a certain instant. Now (2.9) simplifies into

$$(2.11) \quad \begin{aligned} \frac{\partial}{\partial t} \langle Q^2 \rangle + \vec{u} \cdot \nabla \langle Q^2 \rangle - 2 \left(\frac{\partial u}{\partial y} + \frac{\partial v}{\partial x} \right) \langle Q_1 Q_2 \rangle \\ - \left(\frac{\partial u}{\partial x} - \frac{\partial v}{\partial y} \right) \langle Q_1^2 - Q_2^2 \rangle = \frac{8\mathcal{K}\mathcal{T}}{\zeta} - \frac{8HQ_0^2}{\zeta b}. \end{aligned}$$

If using (2.6), the right-hand side of (2.11) can also be written as

$$\frac{4}{\zeta} \left(\frac{2Q_0^2 - (4 + HQ_0^2/\mathcal{K}\mathcal{T}) \langle Q^2 \rangle}{Q_0^2 - 2\langle Q^2 \rangle} \right).$$

Similarly, one may derive the evolution equations for the other second moments $\langle Q_1^2 - Q_2^2 \rangle$ and $\langle Q_1 Q_2 \rangle$. For $\langle Q_1^2 - Q_2^2 \rangle$, we have

$$(2.12) \quad \begin{aligned} \frac{\partial}{\partial t} \langle Q_1^2 - Q_2^2 \rangle + \vec{u} \cdot \nabla \langle Q_1^2 - Q_2^2 \rangle - 2 \left(\frac{\partial u}{\partial y} - \frac{\partial v}{\partial x} \right) \langle Q_1 Q_2 \rangle \\ - \left(\frac{\partial u}{\partial x} - \frac{\partial v}{\partial y} \right) \langle Q^2 \rangle = -\frac{16HQ_0^4\gamma}{\zeta b(b+4)}. \end{aligned}$$

If using (2.8), the right-hand side can also be written as

$$-\frac{4H(Q_0^2 + \langle Q^2 \rangle)}{\zeta(Q_0^2 - 2\langle Q^2 \rangle)} \langle Q_1^2 - Q_2^2 \rangle.$$

For $\langle Q_1 Q_2 \rangle$, we have

$$(2.13) \quad \begin{aligned} \frac{\partial}{\partial t} \langle Q_1 Q_2 \rangle + \vec{u} \cdot \nabla \langle Q_1 Q_2 \rangle - \frac{1}{2} \left(\frac{\partial u}{\partial y} + \frac{\partial v}{\partial x} \right) \langle Q^2 \rangle \\ + \frac{1}{2} \left(\frac{\partial u}{\partial y} - \frac{\partial v}{\partial x} \right) \langle Q_1^2 - Q_2^2 \rangle = -\frac{4HQ_0^4\beta}{\zeta b(b+4)}. \end{aligned}$$

If using (2.7), the right-hand side can also be written as

$$-\frac{4H(Q_0^2 + \langle Q^2 \rangle)}{\zeta(Q_0^2 - 2\langle Q^2 \rangle)} \langle Q_1 Q_2 \rangle.$$

An attractive feature of the moment equations (2.11), (2.12), and (2.13) is that, in absence of the flow field ($\vec{u} = 0$), one can easily see that the system drives the moments $\langle Q^2 \rangle$, $\langle Q_1^2 - Q_2^2 \rangle$, and $\langle Q_1 Q_2 \rangle$ to their equilibrium values $2Q_0^2/(4 + HQ_0^2/\mathcal{KT})$, 0, and 0 exponentially fast. Hence in this case, not only is the equilibrium PDF (1.6) a member of the class (2.1), but it also is a stable attractor of the class.

To complete the moment-closure system coupling the Navier–Stokes equation and the moment equations, one also needs to express the polymeric stress

$$\tau_p = \lambda \int (\nabla_{\vec{Q}} \Psi \otimes \vec{Q}) f d\vec{Q}$$

in terms of the moments $\langle Q^2 \rangle$, $\langle Q_1^2 - Q_2^2 \rangle$, and $\langle Q_1 Q_2 \rangle$. This can also be achieved in the same manner as above by restricting the otherwise general PDF $f(\vec{x}, \vec{Q}, t)$ to the class (2.1). This yields

$$(2.14) \quad \tau_p = \begin{pmatrix} \tau_p^{11} & \tau_p^{12} \\ \tau_p^{21} & \tau_p^{22} \end{pmatrix} = \lambda \begin{pmatrix} \frac{HQ_0^2}{b} + \frac{2HQ_0^4\gamma}{b(b+4)} & \frac{HQ_0^4\beta}{b(b+4)} \\ \frac{HQ_0^4\beta}{b(b+4)} & \frac{HQ_0^2}{b} - \frac{2HQ_0^4\gamma}{b(b+4)} \end{pmatrix}.$$

We see that the effect of γ and β in the ansatz (2.1) is to allow for the existence of different stress components. In the case of horizontal shear flow, we have the normal stress difference $\tau_p^{11} - \tau_p^{22}$ and shear stress τ_p^{12} (or τ_p^{21}), which are responsible for many interesting properties of polymeric fluids. Later, we will also confirm in numerical simulation of driven-cavity flow that keeping both the β and γ terms in our ansatz is essential to preserving the correct flow profile of the FENE fluids. Upon absorbing the HQ_0^2/b term into the pressure by defining

$$(2.15) \quad p' = p - \lambda HQ_0^2/b$$

and using (2.6), (2.7), and (2.8), the polymeric stress less its pressure contribution (still denoted by τ_p) is

$$(2.16) \quad \tau_p = \lambda \frac{H(Q_0^2 + \langle Q^2 \rangle)}{Q_0^2 - 2\langle Q^2 \rangle} \begin{pmatrix} \frac{1}{2} \langle Q_1^2 - Q_2^2 \rangle & \langle Q_1 Q_2 \rangle \\ \langle Q_1 Q_2 \rangle & -\frac{1}{2} \langle Q_1^2 - Q_2^2 \rangle \end{pmatrix}.$$

In summary, we have arrived at a simplified system coupling the Navier–Stokes equation and three moment evolution equations. The significance of this system lies

in that the original Fokker–Planck equation defined on both the spatial and the configuration spaces is replaced by three macroscopic PDEs defined only on the physical space. Using the abbreviations $M_1 = \langle Q^2 \rangle$, $M_2 = \langle Q_1^2 - Q_2^2 \rangle$, and $M_3 = \langle Q_1 Q_2 \rangle$, the proposed moment-closure system can be summarized as follows:

$$(2.17) \quad \frac{\partial \vec{u}}{\partial t} + (\vec{u} \cdot \nabla) \vec{u} + \nabla p' = \lambda \nabla \cdot \left[\frac{H(Q_0^2 + M_1)}{Q_0^2 - 2M_1} \begin{pmatrix} \frac{1}{2}M_2 & M_3 \\ M_3 & -\frac{1}{2}M_2 \end{pmatrix} \right] + \nu \Delta \vec{u},$$

$$(2.18) \quad \nabla \cdot \vec{u} = 0,$$

$$(2.19) \quad \begin{aligned} \frac{\partial}{\partial t} M_1 + \vec{u} \cdot \nabla M_1 - 2 \left(\frac{\partial u}{\partial y} + \frac{\partial v}{\partial x} \right) M_3 - \left(\frac{\partial u}{\partial x} - \frac{\partial v}{\partial y} \right) M_2 \\ = \frac{4}{\zeta} \left(\frac{2Q_0^2 - (4 + HQ_0^2/\mathcal{K}T)M_1}{Q_0^2 - 2M_1} \right), \end{aligned}$$

$$(2.20) \quad \begin{aligned} \frac{\partial}{\partial t} M_2 + \vec{u} \cdot \nabla M_2 - 2 \left(\frac{\partial u}{\partial y} - \frac{\partial v}{\partial x} \right) M_3 - \left(\frac{\partial u}{\partial x} - \frac{\partial v}{\partial y} \right) M_1 \\ = -\frac{4H(Q_0^2 + M_1)}{\zeta(Q_0^2 - 2M_1)} M_2, \end{aligned}$$

$$(2.21) \quad \begin{aligned} \frac{\partial}{\partial t} M_3 + \vec{u} \cdot \nabla M_3 - \frac{1}{2} \left(\frac{\partial u}{\partial y} + \frac{\partial v}{\partial x} \right) M_1 + \frac{1}{2} \left(\frac{\partial u}{\partial y} - \frac{\partial v}{\partial x} \right) M_2 \\ = -\frac{4H(Q_0^2 + M_1)}{\zeta(Q_0^2 - 2M_1)} M_3. \end{aligned}$$

These equations are coupled with proper boundary conditions and initial conditions to be specified depending on the problems under consideration.

3. Energy estimates and local existence. To understand the structure of the closure system (2.17)–(2.21) in a bounded spatial domain Ω , we now consider the local well-posedness under the boundary condition $\vec{u} = 0$ on the boundary $\partial\Omega$ of Ω . For simplicity, we assume that $\partial\Omega$ is sufficiently smooth. Some relevant analytical work on the original micro-macro coupled system can be found in [19, 10]. However, their methods are different from what we use here.

Under the homogeneous boundary condition for \vec{u} , the original system (1.1)–(1.3) enjoys the following energy estimate, independent of the form of the potential Ψ :

$$(3.1) \quad \begin{aligned} \frac{d}{dt} \int \left(\frac{1}{2} |\vec{u}|^2 + \lambda \int (\mathcal{K}T f \ln f + \Psi f) dQ \right) dx \\ = - \int \left(\nu |\nabla \vec{u}|^2 + \frac{2\lambda}{\zeta} \int f |\nabla_Q (\mathcal{K}T \ln f + \Psi)|^2 dQ \right) dx. \end{aligned}$$

One major advantage of the moment-closure procedure given in the previous section is that the new system (2.17)–(2.21) still possesses the following energy law analogous to (3.1):

$$(3.2) \quad \begin{aligned} \frac{d}{dt} \int \left(\frac{1}{2} |\vec{u}|^2 + \lambda G(M_1) \right) dx \\ = - \int \left(\nu |\nabla \vec{u}|^2 + \frac{4\mathcal{K}T}{\zeta} \left(\frac{2Q_0^2 - (4 + HQ_0^2/\mathcal{K}T)M_1}{Q_0^2 - 2M_1} \right) \frac{H(Q_0^2 + M_1)}{Q_0^2 - 2M_1} \right) dx \\ = - \int \left(\nu |\nabla \vec{u}|^2 + \frac{4HQ_0^2}{\zeta M_1(Q_0^2 - 2M_1)} \frac{H(Q_0^2 + M_1)}{Q_0^2 - 2M_1} - \frac{8\mathcal{K}T}{\zeta} \frac{H(Q_0^2 + M_1)}{Q_0^2 - 2M_1} \right) dx, \end{aligned}$$

where $G(M_1) = -\frac{1}{4}HM_1 - \frac{3}{8}HQ_0^2 \ln(1 - 2M_1/Q_0^2)$ is a scalar function such that $G'(M_1) = H(Q_0^2 + M_1)/(2Q_0^2 - 4M_1)$. This energy law also illustrates the special coupling between the transport of M_1 and the elastic stress in the momentum equation.

Notice that the derivation of the energy law (3.2) does not involve the equation of M_2 and M_3 . In fact, using the distribution (1.6), we see that the original elastic energy $\int \Psi f dQ = HM_1/(1 - M_1/Q_0^2)$. Comparing this with $G(M_1)$, we see that the leading linear terms are the same as $HM_1/2$, and they differ only from the quadratic and higher order terms. Hence in the case that M_1 is close to the equilibrium $2Q_0^2/(4 + HQ_0^2/\mathcal{KT})$, the new closure system is very close to the original system from the energy point of view. When looking at the terms involving the thermotemperature \mathcal{KT} , we see that in (3.2) it is the only term that may not be dissipative. Also, in the equations of M_2 and M_3 , when \mathcal{KT} is zero, the right-hand side terms lose their damping property. This may well be the main reason that our method can work only in certain cases.

To study the well-posedness of the system (2.17)–(2.21), we set the new variable $U = (\vec{u}^T, M_1 - 2Q_0^2/(4 + HQ_0^2/\mathcal{KT}), M_2, M_3)^T = (\vec{u}^T, U'^T)^T$. We see that (2.17)–(2.21) is a quasi-linear system in U . The main difficulty of the system is the lack of dissipation to the M_i part of U . However, we notice that all the right-hand sides of the M_i equations, denoted by $B(U')$, have a damping effect, at least in the case that $M_1 - 2Q_0^2/(4 + HQ_0^2/\mathcal{KT})$ is small.

Moreover, we notice that when $\nu = 0$ the system is in fact a symmetric hyperbolic system in (\vec{u}, M_1) , although we do not have the same property with M_2 and M_3 .

Let $|\cdot|_k$ be the Sobolev seminorm and $\|\cdot\|_k$ be the Sobolev norm. For all integer sets $\alpha = (\alpha_1, \alpha_2)$, we also write $\nabla_x^{\alpha_1} \nabla_y^{\alpha_2}$ as ∇^α . For all possible $|\alpha| \leq k$, we can take ∇^α of the U' equations in the system, multiply by $\nabla^\alpha U'$, and integrate over the domain Ω . We have

$$\frac{1}{2} \frac{d}{dt} |\nabla^\alpha U'|^2 \leq |(\nabla^\alpha(\vec{u} \cdot \nabla U'), \nabla^\alpha U')| + C(|(\nabla^\alpha(\nabla \vec{u} U'), \nabla^\alpha U')| + (\nabla^\alpha(B(U')), \nabla^\alpha U')).$$

We can easily estimate the right-hand side terms individually:

$$\begin{aligned} & |(\nabla^\alpha(\vec{u} \cdot \nabla U'), \nabla^\alpha U')| \\ &= |(\nabla^\alpha(\vec{u} \cdot \nabla U') - \vec{u} \cdot \nabla \nabla^\alpha U', \nabla^\alpha U')| \\ &\leq |\vec{u}|_\alpha |\nabla U'|_\infty |U'|_\alpha + |\nabla \vec{u}|_\infty |U'|_\alpha^2, \end{aligned}$$

where we have used the divergence-free condition $\nabla \cdot \vec{u} = 0$ and the zero boundary condition for \vec{u} . We also have

$$\begin{aligned} & |(\nabla^\alpha(\nabla \vec{u} U'), \nabla^\alpha U')| \leq |\vec{u}|_{\alpha+1} |U'|_\infty |U'|_\alpha + |\nabla \vec{u}|_\infty |U'|_\alpha^2, \\ & |(\nabla^\alpha(B(U')), \nabla^\alpha U')| \leq A(|U'|_\infty) \|U'\|_\alpha^2, \end{aligned}$$

where $A(\cdot)$ is an algebraic function. Similarly, from the momentum equation of the velocity, together with $\nabla \cdot \vec{u} = 0$, one may derive using standard techniques of higher-order energy estimates for the Navier–Stokes equations¹

$$\frac{1}{2} \frac{d}{dt} |\vec{u}|_\alpha^2 + \nu |\vec{u}|_{\alpha+1}^2 \leq C(|\nabla \vec{u}|_\infty |\vec{u}|_\alpha^2 + |U'|_\infty |\vec{u}|_\alpha \|U'\|_\alpha).$$

¹For instance, using a Galerkin approach [21, 30], one may decompose the fluid velocity \vec{u} in the space of eigenfunctions of the Stokes operator with the homogeneous Dirichlet boundary condition. Then the zero boundary condition for \vec{u} induces zero boundary conditions for suitable combinations of the higher-order derivatives of \vec{u} and the pressure and simplifies the results of integration by parts.

Combining these estimates, we arrive at

$$\begin{aligned} & \frac{d}{dt} \left(\frac{1}{2} |\bar{u}|_\alpha^2 + \frac{1}{2} |U'|_\alpha^2 \right) + \nu |\bar{u}|_{\alpha+1}^2 \\ & \leq C (|\bar{u}|_\alpha |\nabla U'|_\infty |U'|_\alpha + |\nabla \bar{u}|_\infty |U'|_\alpha^2 + |\bar{u}|_{\alpha+1} |U'|_\infty |U'|_\alpha \\ & \quad + |\nabla \bar{u}|_\infty |U'|_\alpha^2 + |\nabla \bar{u}|_\infty |\bar{u}|_\alpha^2 + |U'|_\infty |\bar{u}|_\alpha \|U'\|_\alpha) + A(|U'|_\infty) \|U'\|_\alpha^2. \end{aligned}$$

We can further sum up to k for all α . If $k \geq 3$, by Sobolev embedding theorems we have that $|\nabla \cdot |_\alpha \leq \| \cdot \|_k$. Hence, using the Schwartz inequality we have that

$$\begin{aligned} (3.3) \quad & \frac{1}{2} \frac{d}{dt} (\|\bar{u}\|_k^2 + \|U'\|_k^2) + \frac{\nu}{2} \|\bar{u}\|_{k+1}^2 \\ & \leq C \left(\|\bar{u}\|_k^2 + \frac{1}{2} \|U'\|_k^2 \right)^2 + A(|U'|_\infty) \|U'\|_k^2. \end{aligned}$$

We can then apply a standard procedure [21] to get the following local existence of a classical solution.

THEOREM 3.1. *Given an integer $k \geq 3$, $\bar{u}_0 \in H_0^1(\Omega) \cap H^k(\Omega)$, $M_i \in H^k(\Omega)$, then there exists a positive time T such that the system (2.17)–(2.21) has a unique solution $\bar{u}(t, x) \in L^\infty(0, T; H^k(\Omega)) \cap L^2(0, T; H^{k+1}(\Omega))$, $M_i \in L^\infty(0, T; H^k(\Omega))$. Moreover, if T^* is the maximal time of existence, then*

$$\int_0^{T^*} \left(|\nabla \bar{u}(\cdot, s)|_{L^\infty(\Omega)} + \sum_1^3 |\nabla M_i(\cdot, s)|_{L^\infty(\Omega)} \right) + A(|M_i|_\infty) ds = +\infty.$$

Moreover, if we can guarantee that the right-hand sides of (2.19)–(2.21) have a pure damping effect (such as in the case that $M_1 - 2Q_0^2/(4 + HQ_0^2/\mathcal{K}T)$ is small), that is, we have that

$$(\nabla^\alpha(B(U')), \nabla^\alpha U') \geq \delta |U'|_\alpha^2 > 0,$$

then the estimate (3.3) in fact gives the global existence of a classical solution when the initial data is small.

THEOREM 3.2. *Given an integer $k \geq 3$, let $\bar{u}_0 \in H_0^1(\Omega) \cap H^k(\Omega)$, $M_i \in H^k(\Omega)$ for $i = 1, 2, 3$. For any given viscosity constant μ , if we have $\|\bar{u}_0\|_k$, $\|M_1 - 2Q_0^2/(4 + HQ_0^2/\mathcal{K}T)\|_k$, $\|M_2\|_k$, and $\|M_3\|_k$ small enough, then there exists a unique global solution of the closure system (2.17)–(2.21) such that $\bar{u}(t, x) \in L^\infty(0, T; H^k(\Omega)) \cap L^2(0, T; H^{k+1}(\Omega))$, $M_i \in L^\infty(0, T; H^k(\Omega))$ for any fixed time T .*

We point out that the nonlinearities in the transport part of the M_i equations are the same as in the usual Oldroyd models [5]. In the small datum case, the right-hand side terms provide the damping dissipation. It will be interesting if one can get the global weak solution using the energy law (3.2). Intuitively, this is also related to how the thermoentropy in the original energy law affects the closure system. Such an issue will be studied in our future work.

4. Numerical results: Steady shear flow. In what follows, we will investigate the use of numerical simulations to validate the moment-closure approximation on two types of flow problems: simple shear flow and driven-cavity flow. This section is concerned with the solution to the moment equations under the influence of steady shear flow. For comparison purposes, it is feasible to solve the Fokker–Planck equation (1.3) directly because there is no need for flow calculation in the present case. The

full system coupling the Navier–Stokes equations and the Fokker–Planck or moment equations will be considered in the next section. Our goal here is to examine the closeness of our moment-closure approximation to the exact solution of the Fokker–Planck equation under the influence of increasing shear rates.

Suppose $\vec{u} = (\kappa y, 0)$, where κ is the constant shear rate. Due to the spatially uniform shear rate, the Fokker–Planck equation reduces to a PDE only in the configuration space of \vec{Q} ,

$$(4.1) \quad \frac{\partial f(\vec{Q}, t)}{\partial t} + \frac{\partial}{\partial Q_1}(\kappa \vec{Q}_2 f) = \frac{2}{\zeta} \nabla_{\vec{Q}} \cdot (\nabla_{\vec{Q}} \Psi f) + \frac{2\mathcal{K}\mathcal{T}}{\zeta} \Delta_{\vec{Q}} f.$$

Since the spatial dependence of f is absent, we can afford to simulate the Fokker–Planck equation directly. We use a finite-difference scheme that exploits the probabilistic nature of the equation. To avoid singularity of the FENE force law near the boundary of the probability space $|\vec{Q}| = Q_0$, we solve the Fokker–Planck equation in a smaller domain with an artificial boundary at $|Q| = Q_0 - \epsilon$. The domain is discretized on an $M \times M$ regular grid covering the square $\{\vec{Q} \mid Q_1 < Q_0 \text{ and } Q_2 < Q_0\}$ with mesh size $h = 2Q_0/M$, while the constraint $|\vec{Q}| < Q_0 - \epsilon$ is taken into account by setting only the grid points satisfying this constraint active in the computation. If the PDF is well concentrated around the origin, as in the case of moderate velocity gradient, the difference between the solution on the restricted domain and the actual solution is negligibly small. For a certain grid point (i, j) , the discrete probability $P_{i,j}^n$, where n denotes the current time step, is updated by means of a discrete analogue of the Chapman–Kolmogorov equation

$$(4.2) \quad P_{i,j}^n = (1 - \Gamma_{i,j}^{i-1,j} - \Gamma_{i,j}^{i+1,j} - \Gamma_{i,j}^{i,j-1} - \Gamma_{i,j}^{i,j+1})P_{i,j}^{n-1} + \Gamma_{i,j-1}^{i,j}P_{i,j-1}^{n-1} + \Gamma_{i,j+1}^{i,j}P_{i,j+1}^{n-1} + \Gamma_{i-1,j}^{i,j}P_{i-1,j}^{n-1} + \Gamma_{i+1,j}^{i,j}P_{i+1,j}^{n-1},$$

where $\Gamma_{i,j}^{k,l}$ represents the transition probability from the grid point (i, j) to (k, l) during one time step. The transition probabilities $\Gamma_{i,j}^{k,l}$ are determined such that the Chapman–Kolmogorov equation approaches the Fokker–Planck equation in the continuum limit as the mesh size $h \rightarrow 0$; that is, (4.2) gives a consistent approximation to (4.1). The no-flux boundary condition can be readily implemented by setting those transition probabilities to or from grid points violating the constraint $|\vec{Q}| < Q_0 - \epsilon$ to zero. The advantage of this scheme is that, given appropriate stability constraints on time and spatial step sizes such that the transition probabilities $\Gamma_{i,j}^{i,j-1}$, $\Gamma_{i,j}^{i,j+1}$, $\Gamma_{i,j}^{i-1,j}$, and $\Gamma_{i,j}^{i+1,j}$ are all in the range of $[0, 1]$ (more details are given in [8]), the positivity and the unity ($\sum_{i,j} P_{i,j}^n = 1$) of the discrete probability $P_{i,j}^n$ are automatically preserved. The consistency and stability together will ensure the convergence of the numerical approximation.

In all our computations, a 500×500 grid is used in the configuration space which is fine enough to resolve the solutions of (4.1) in the parameter regime of interests here. The results obtained by solving (4.2) can be compared with those obtained from solving the moment equations. In the case of simple shear flow, the moment equations (2.19)–(2.21) reduce to the following ODEs:

$$(4.3) \quad \frac{d}{dt} M_1 - 2\kappa M_3 = \frac{4\mathcal{K}\mathcal{T}}{\zeta} \left(\frac{2Q_0^2 - (4 + H Q_0^2/\mathcal{K}\mathcal{T})M_1}{Q_0^2 - 2M_1} \right),$$

$$(4.4) \quad \frac{d}{dt} M_2 - 2\kappa M_3 = -\frac{4H(Q_0^2 + M_1)}{\zeta(Q_0^2 - 2M_1)} M_2,$$

$$(4.5) \quad \frac{d}{dt}M_3 - \frac{1}{2}\kappa M_1 + \frac{1}{2}\kappa M_2 = -\frac{4H(Q_0^2 + M_1)}{\zeta(Q_0^2 - 2M_1)}M_3.$$

Recall that each triplet (M_1, M_2, M_3) uniquely determines a distribution function in the class (2.1), and the detailed PDF obtained from solving the moment system (4.3)–(4.5) can thus be compared with that from solving the Fokker–Planck equation directly. Since in general the influence on flow is exerted through the polymeric stress τ_p , we will also compare the polymeric stresses obtained from solving the Fokker–Planck equation and the moment equations, respectively.

The physical parameters used in the simulations here are $\zeta = 40$, $\mathcal{K}T = 1$, $H = 100$, and $Q_0 = 1$, as will be used in the next section for the driven-cavity flow. For each choice of κ , the Fokker–Planck equation and the moment-closure system are solved numerically until equilibrium is reached when we measure the PDFs and the polymeric stresses. First, we present the comparison between the equilibrium PDFs for $\kappa = 1, 3$, and 6 in Figure 4.1, in which the contour lines of the PDFs are plotted. We see that for small $\kappa = 1$ the two distributions are very similar, illustrating that (2.1) is a good approximation to the true PDF for small perturbation of the equilibrium PDF. As the shear rate increases to $\kappa = 3$, the PDF (2.1) determined from the moment-closure simulation displays an apparently distinct shape from the actual distribution. However, as shown by the data to be presented next, the stresses corresponding to the two distributions still agree perfectly. This manifests nicely the philosophy behind our moment-closure approach. Namely, the important degrees of freedom are captured, although the fully detailed distribution space is not completely reproduced. For $\kappa = 6$, the ansatz (2.1) has ceased to be a meaningful PDF as it takes negative values somewhere, as marked on the picture at the nonconvex region of the contours. Despite the fact that (2.1) can no longer be interpreted as a PDF, the moment equations (4.3)–(4.5) are still well defined, from which the steady-state values of the moments can be calculated.

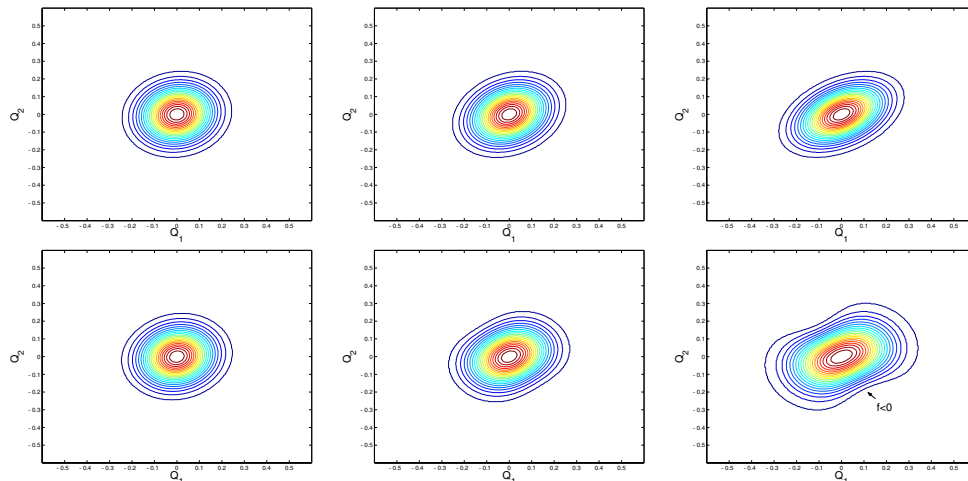


FIG. 4.1. Comparison of the contour plots of the PDFs solved from the Fokker–Planck equation (top row) and the moment equations (bottom row) for $\kappa = 1, 3$, and 6 .

We next present the comparison of the stresses obtained from the Fokker–Planck equation and the moment equations for a wide range of shear rate $\kappa \in [1, 20]$. Figure 4.2 plots the normal stress and shear stress obtained by the Fokker–Planck and

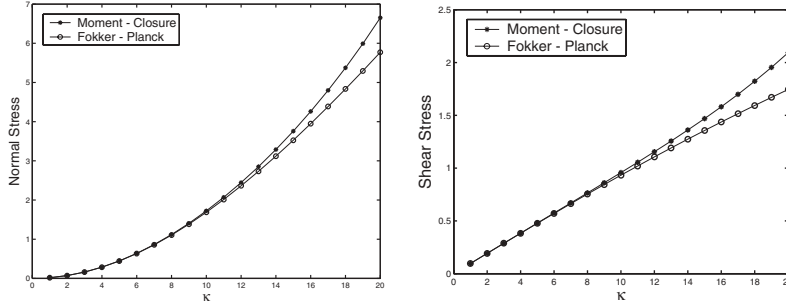


FIG. 4.2. Comparison of the normal stress (left) and the shear stress (right) by solving Fokker-Planck and moment equations.

moment-closure equations, respectively. Surprisingly, the agreement is excellent for $\kappa < 10$, which is well beyond the regime of κ for which the ansatz (2.1) can be interpreted as a PDF. As κ becomes larger than 10, the moment-closure approximation starts to deviate appreciably from the true stresses. This gives an indication of the validity and applicability of our moment-closure approach to more realistic simulation of the coupled system (2.17)–(2.21).

To understand the new closure approximation from the energy point of view, we also compare the elastic energy $\int \Psi f dQ$ by solving the Fokker-Planck equation and its counterpart $G(M_1) = -\frac{1}{4}HM_1 - \frac{3}{8}HQ_0^2 \ln(1 - \frac{2M_1}{Q_0^2})$ by solving the moment equations. The result is shown in Figure 4.3. We see a similar pattern observed for the comparison between the polymeric stresses. Namely, the two energy forms agree well for small shear rates, while they start to deviate significantly for larger κ . This observation confirms from the perspective of the energy law that our moment-closure procedure with the ansatz (2.1) may be viewed as a perturbation approach and is expected to be valid only when the distorted configuration space does not differ too much from the equilibrium PDF.

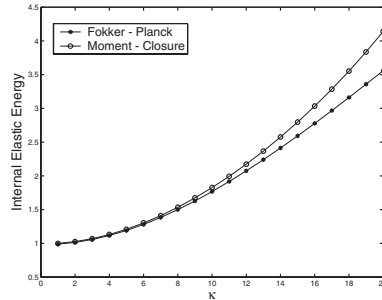


FIG. 4.3. Comparison of the elastic energies corresponding to the original Fokker-Planck equation and the simplified moment equations.

5. Numerical results: The coupled system. We now present numerical simulations on the coupled moment-closure system (2.17)–(2.21) in comparison with the original model (1.1)–(1.3).

We take on a square domain $[0, 1] \times [0, 1]$. The no-flow boundary condition $\vec{u} \cdot \vec{n} = 0$ is imposed at all boundaries. Consequently, there is no need to impose boundary

conditions for $f(\cdot, Q, t)$ in the case of the original system and for M_1 , M_2 , and M_3 in the case of the moment-closure system. Different ways to prescribe the tangential components of the boundary velocities will be explored, including a regularized driven-cavity flow problem. We will solve the moment-closure system and compare the results against those obtained from solving the original system by a Monte Carlo approach.

5.1. Description of algorithms. The main components of the simulation algorithms include a Navier–Stokes solver, coupled with a solver for the equations of moments and a Monte Carlo code for simulating the stochastic dynamics.

Navier–Stokes solver. The momentum equation ((1.1) or (2.17)) is solved using a simple second-order finite-difference scheme based on vorticity-stream function formulation, as described in E and Liu [9]. Introducing the vorticity $\omega = \nabla \times \vec{u}$ and the stream function ψ such that $\vec{u} = (-\frac{\partial\psi}{\partial y}, \frac{\partial\psi}{\partial x})$, the two-dimensional (2D) vorticity-stream function formulation reads

$$(5.1) \quad \begin{cases} \frac{\partial\omega}{\partial t} + (\vec{u} \cdot \nabla)\omega = \nu \Delta \omega + \nabla \times (\nabla \cdot \tau_p), \\ \Delta\psi = \omega. \end{cases}$$

The Poisson equation $\Delta\psi = \omega$ is solved with the homogeneous Dirichlet boundary condition. The equation for ω is solved only in the interior, and the boundary values of ω are updated using the Thom’s formula.

The system (5.1) is discretized on a uniform grid with spatial differential operators replaced by standard center differencing formulas, except that the $\nabla \times (\nabla \cdot \tau_p)$ term at grid points immediately adjacent to the boundary is approximated using one-sided differencing formulas constructed to ensure local second-order accuracy. The use of one-sided differencing for the polymer stress τ_p near the boundary is entailed by the lack of boundary condition for the Fokker–Planck equation, and hence the lack of boundary condition for the moment equations.

Since we are mainly interested in small viscosity solutions, explicit time stepping can be used with a convectively stable time stepping procedure such as the fourth-order Runge–Kutta. In the absence of the extra force term $\nabla \times (\nabla \cdot \tau_p)$, the scheme is fourth-order accurate in time if the Poisson equation is solved four times for each time step, once per Runge–Kutta update. However, due to the coupling of the Navier–Stokes equation and the Fokker–Planck or moment equations, the polymer stress τ_p will be updated only once for each time step for efficiency considerations. This leads to a first-order scheme in time.

Outlined below is the algorithm to solve the Navier–Stokes equations via the vorticity-stream function formulation. The polymeric stress τ_p is determined either by a Monte Carlo simulation of the Fokker–Planck equation or by solving the moment equations, the details of which will be described later. Given ω^n up to the boundary and the current polymer stress τ_p^n in the interior, the following steps are taken:

1. Update ω^{n+1} in the interior by solving the equation for ω in (5.1) using the fourth-order Runge–Kutta.
2. Solve the discretized Poisson equation $\nabla_h \psi^{n+1} = \omega^{n+1}$ using FFT with the homogeneous Dirichlet boundary condition.
3. Update ω^{n+1} at the boundary using the Thom’s formula.
4. Update the polymeric stress τ_p^{n+1} by either Monte Carlo simulation or the moment equations.

Monte Carlo code. Due to the difficulty in fully resolving the configuration space, a popular approach is to replace the Fokker–Planck equation (1.3) by Monte Carlo

simulation of its underlying stochastic differential equation. In the Brownian configuration field (BCF) method [17], the stochastic equation to solve is

$$(5.2) \quad d\vec{Q} + \vec{u} \cdot \nabla \vec{Q} dt = \left(\nabla \vec{u} \vec{Q} - \frac{2}{\zeta} \nabla_{\vec{Q}} \Psi \right) dt + \sqrt{\frac{4\mathcal{K}\mathcal{T}}{\zeta}} dW_t,$$

where W_t is a standard 2D Brownian motion *independent* of the spatial variable \vec{x} . It is a novel feature of the BCF to choose a spatially uniform noise term, which can be thought of as a technique of variance reduction [27]. In Monte Carlo simulations, a large number of Brownian fields $Q_i(\vec{x}, t)$, where $i = 1, \dots, N$, are simulated independently using (5.2), and the polymer stress τ_p is approximated by an ensemble average,

$$\tau_p = \frac{1}{N} \sum_{i=1}^N (\nabla_{\vec{Q}} \Psi(\vec{Q}_i) \otimes \vec{Q}_i).$$

Special care has to be given in order to ensure the finite extensibility constraint $|\vec{Q}| < Q_0$. To circumvent the possibility of illegal $|\vec{Q}|$ values, we adopt the semi-implicit predictor-corrector scheme of Ottinger [26] with a slight generalization to include the convective term. Given \vec{u}^n, \vec{Q}^n at time t_n , the predictor step is to apply the Euler–Maruyama scheme to compute an intermediate value \vec{Q}^* ,

$$(5.3) \quad \vec{Q}^* = \vec{Q}^n + \left(-\vec{u}^n \cdot \nabla \vec{Q}^n + \nabla \vec{u}^n \vec{Q}^n - \frac{2}{\zeta} \nabla_{\vec{Q}} \Psi(\vec{Q}^n) \right) \Delta t + \sqrt{\frac{4\mathcal{K}\mathcal{T}}{\zeta}} \Delta W,$$

where ΔW is a 2D Gaussian random variable whose components have variance Δt . We recall that the force term $\nabla_{\vec{Q}} \Psi = H\vec{Q}/(1 - (Q/Q_0)^2)$. The corrector step that determines \vec{Q}^{n+1} at time $t_{n+1} = t_n + \Delta t$ treats only the force term implicitly and reads

$$(5.4) \quad \left[1 + \frac{H\Delta t}{\zeta(1 - (\frac{Q^{n+1}}{Q_0})^2)} \right] \vec{Q}^{n+1} = \vec{Q}^n - \frac{1}{2} [\vec{u}^{n+1} \cdot \nabla \vec{Q}^* + \vec{u}^n \cdot \nabla \vec{Q}^n] \Delta t + \frac{1}{2} \left[\nabla \vec{u}^{n+1} \vec{Q}^* + \nabla \vec{u}^n \vec{Q}^n - \frac{2H\vec{Q}^n}{\zeta(1 - (\frac{Q^n}{Q_0})^2)} \right] \Delta t + \sqrt{\frac{4\mathcal{K}\mathcal{T}}{\zeta}} \Delta W.$$

Notice the same random number is used in (5.3) and (5.4). The length of \vec{Q}^{n+1} can be determined from a cubic equation which, for arbitrary length of the vector on the right-hand side of (5.4), has a unique solution between 0 and $\sqrt{Q_0}$. Thus, the scheme automatically guarantees the finite extensibility constraint.

Finally, we discuss the spatial discretization of the gradient terms in (5.3) and (5.4). While a straightforward center differencing for ∇u is used, the convective terms of the form $\vec{u} \cdot \nabla \vec{Q}$ require some special treatment due to the lack of boundary condition for \vec{Q} . Recall the notation $\vec{u} = (u, v)$ and $\vec{Q} = (Q_1, Q_2)$. Let us discuss only the treatment of $u \frac{\partial Q_1}{\partial x}$ at a grid point (i, j) . Suppose i is the horizontal index, and $u \frac{\partial Q_1}{\partial x}$ is approximated by

$$(5.5) \quad \left(u \frac{\partial Q_1}{\partial x} \right)_{i,j} \approx u_{i-1,j} \frac{Q_1^{i,j} - Q_1^{i-1,j}}{2h} + u_{i+1,j} \frac{Q_1^{i+1,j} - Q_1^{i,j}}{2h}.$$

At grid points immediately adjacent to the boundary, this formula together with the no-flow boundary condition automatically selects the correct differencing direction to avoid using values of Q_1 on the boundary.

Solver for the moment equations. Many of the numerical issues worth noticing for the solution of the moment equations (2.19)–(2.21) have been encountered in the above discussion of the Navier–Stokes equation and the Monte Carlo simulation. More specifically, we treat components of $\nabla\vec{u}$ by center differencing, and we treat the convective terms of the form $\vec{u}\cdot\nabla M_i$ in the same way as (5.5). Explicit time stepping with the fourth-order Runge–Kutta is taken for convenience. We note, however, that it is possible to develop a discretization scheme that would preserve a discrete energy law similar to (3.2). Furthermore, due to the lack of diffusion terms in the moment equations, it is also possible to apply an upwinding scheme in place of (5.5) for better numerical stability.

5.2. Simulation results. We simulate the original system and the moment-closure system on the domain $[0, 1] \times [0, 1]$ with various slip boundary conditions. The goal is to compare in detail the flow patterns and the polymeric stresses produced by the original and simplified models.

To reduce the number of physical parameters, we first identify the scaling properties of the original system and the moment-closure system. In both systems, the scales of the boundary velocity, temperature and Q_0 can be absorbed into other parameters, and the remaining independent physical parameters are polymer density λ , the fluid viscosity ν , the friction coefficient ζ , and the elasticity constant H . So, the maximum boundary velocity is taken to be unity in all of our numerical experiments, and we let $\mathcal{KT} = Q_0 = 1$. In our first set of numerical experiments, we choose the other physical parameters to be $\lambda = 0.05$, $\nu = 10^{-3}$, $\zeta = 40$, and $H = 100$. Some comments on other choices of the physical parameters will be made at the end of this section.

Driven-cavity flow. We first consider a driven-cavity problem. The driven-cavity problem has been a standard test problem for numerical schemes designed to solve the incompressible Navier–Stokes equations. However, to the best of our knowledge, there have been no results available in the literature on driven-cavity flow of the FENE fluids. Thus, we validate our moment-closure model against the Monte Carlo simulation. We adopt a similar boundary condition as in [9]: $u(x, y = 1, t) = 16a(t)x^2(1-x)^2$, and boundary velocities elsewhere are zeros. We model the start-up flow with the time-dependent factor $a(t) = 0.1t$ for $t < 10$ and $a(t) = 1$ for $t \geq 10$. Initially, the fluid is at rest. The initial dumbbell configuration in the Monte Carlo simulation is generated from the equilibrium PDF (1.6).

Since the Monte Carlo simulation is computationally very demanding, the comparison of the moment-closure and Monte Carlo results is produced on a 50×50 grid. On the other hand, we have checked that refining the grid to 200×200 for the moment-closure system results only in a 3 percent relative error for the computed equilibrium stream function measured in the L^∞ norm. The discrete time step is taken to be $\Delta t = 10^{-3}$ to ensure the stability and the accuracy of the simulation, and computational results at $t = 50$ are presented, when the numerical solutions appear to have reached equilibrium.

The left picture in Figure 5.1 presents the contour plots of the stream functions in the moment-closure and Monte Carlo calculations on the same coordinate system. The two contour plots are nearly indistinguishable. The Monte Carlo stream function is obtained by averaging over 100 independent simulation runs, each of which employs 100 BCFs. We also present in Figure 5.1 the contour plot of the stream function for

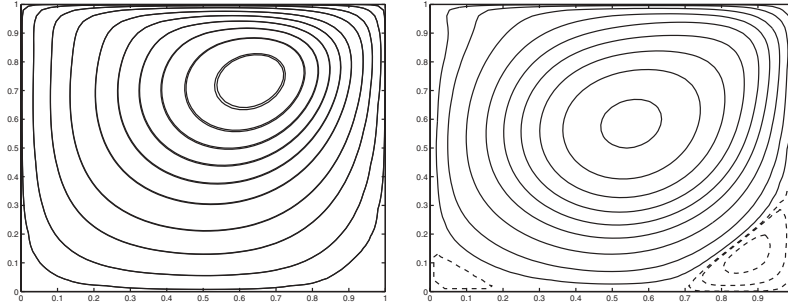


FIG. 5.1. Contour plots of the stream functions at $t = 50$ in the moment-closure and Monte Carlo simulations (left) and in the Newtonian flow by solving the Navier–Stokes equations (right).

the Newtonian flow obtained by solving the Navier–Stokes equations free from the effect of the polymeric stress. The fact that the Newtonian flow develops vortices at the lower left and right corners that are not present in the non-Newtonian case indicates a strong smoothing effect by the polymeric stress in our sample calculation. We also compare the polymeric stress at $t = 50$ in the moment-closure and Monte Carlo simulations. The left column of Figure 5.2 shows the contour plots of the normal and shear stress (defined as $\tau_p^{11} - \tau_p^{22}$ and $\tau_p^{12} = \tau_p^{21}$, respectively) obtained from the Monte Carlo simulation, while the right column shows the results from the moment-closure calculation. The agreement is very good.

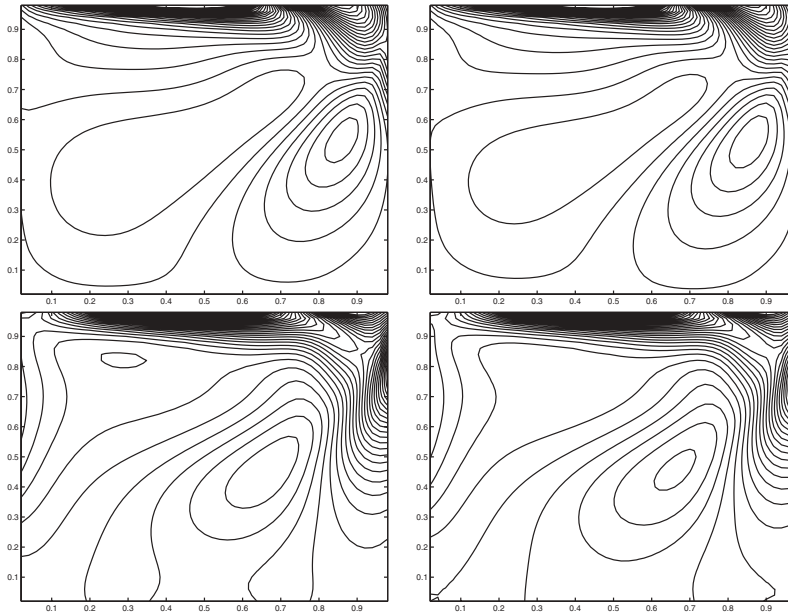


FIG. 5.2. Contour plots of the polymeric normal (top) and shear (bottom) stresses in the Monte Carlo (left) and moment-closure simulations (right).

We introduce several quantitative measurements on the statistical error of the Monte Carlo simulation and on the closeness of the moment-closure approximation. First, we denote averaged quantities over the 100 independent Monte Carlo simulation

runs by a star; e.g., ψ^* represents the averaged stream function. For a quantity of interest ϕ (maybe stream function, moments, stresses, etc.), we define σ , the standard deviation in the L^∞ norm of the Monte Carlo simulation relative to $\|\phi^*\|_\infty$, as

$$\sigma = \sqrt{\frac{1}{N-1} \sum_{i=1}^N \frac{\|\phi_i - \phi^*\|_\infty^2}{\|\phi^*\|_\infty^2}},$$

where $N = 100$ is the total number of Monte Carlo runs. Denoting by $\tilde{\phi}$ the moment-closure approximation to ϕ , we define e , the relative error, as

$$e = \|\tilde{\phi} - \phi^*\|_\infty / \|\phi^*\|_\infty.$$

Table 5.1 lists the standard deviation of the Monte Carlo simulation and relative error of the moment-closure approximation for such quantities as the stream function, moments, and components of the polymeric stress at $t = 50$. We see that for the stream function, the error committed by the moment-closure approximation is so small that it is even within the statistical error of the Monte Carlo simulation employing 100 BCFs. Another significant result is that, for the moments and stresses, the error of the moment-closure approximation is one magnitude smaller than the statistical error of the Monte Carlo simulation. This indicates that in order for the Monte Carlo simulation to achieve the same level of statistical error as the accuracy of the moment-closure method in computing the polymeric stress, as many as 10,000 BCFs need to be used. However, even with just 100 Brownian fields, the Monte Carlo simulation typically takes 30 times as much running time as the moment-closure approach. So at least for the current test problem of driven-cavity flow, the savings and accuracy of the moment-closure approach prove to be very satisfactory.

TABLE 5.1

Standard deviations of the Monte Carlo simulation and errors of the moment-closure approximation. ψ : stream function. M_i ($i = 1, 2, 3$): moments. $\tau_p^{11} + \tau_p^{22}$: polymeric pressure. $\tau_p^{11} - \tau_p^{22}$: normal stress. $\tau_p^{12} = \tau_p^{21}$: shear stress.

	ψ	M_1	M_2	M_3	$\tau_p^{11} + \tau_p^{22}$	$\tau_p^{11} - \tau_p^{22}$	$\tau_p^{12} = \tau_p^{21}$
σ	2.7%	12.7%	19.5%	26.0%	13.7%	20.2%	25.8%
e	1.1%	1.4%	1.1%	2.7%	0.9%	1.5%	2.7%

We make a brief comment on the counterintuitive fact reflected in the table that the huge standard deviation of the polymeric stress in the Monte Carlo simulation does not seem to deteriorate the moderate statistical error of the stream function ψ . A closer look at the components of the stress tensor produced by the Monte Carlo simulation reveals that the shapes of the stress profiles compare well among independent Monte Carlo runs, but a shift by a random constant can be clearly seen. However, the constant shift does not contribute to the calculation of the flow upon taking the divergence. This observation is consistent with those in Bonvin and Picasso [3] and manifests a specific manner in which the BCF method achieves variance reduction.

To conclude our first numerical test on the driven-cavity problem, we show that the excellent agreement of the moment-closure approach with the Monte Carlo result is not a pure coincidence but is in fact contingent upon the basic ansatz (2.1) from which our moment-closure method is derived. For this purpose, two other reduced moment-closure systems are derived by simply imposing $\beta = 0$ or $\gamma = 0$ in (2.1),

respectively. In the case of horizontal shear flow, the assumption $\beta = 0$ amounts to enforcing zero shear stress but allowing normal stress to exist, and the assumption $\gamma = 0$ corresponds to enforcing zero normal stress but allowing shear stress to exist. The associated moment-closure systems can be derived similarly and are in fact simple reductions of the moment-closure system (2.17)–(2.21). Figure 5.3 shows the contour plots of the stream functions obtained from the two reduced moment-closure systems at $t = 50$, otherwise with the same physical parameters and boundary conditions. We see that ignoring either the β term or the γ term in the ansatz (2.1) would lead to dramatically different flow than the correct result in Figure 5.1. Furthermore, it seems that the normal component of the polymeric stress tensor plays a relatively more important role than the shear component in preserving the correct flow profile.

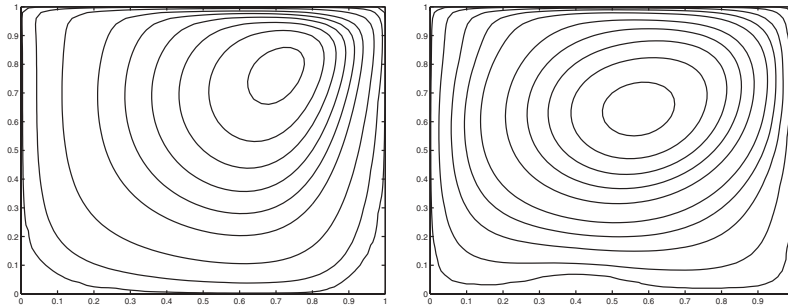


FIG. 5.3. Stream function in the reduced moment-closure approximation allowing only normal stress (left) or only shear stress (right). $t = 50$.

Other boundary conditions. We have also tested the moment-closure method on four other types of boundary conditions: (1) $u = 16a(t)x^2(1-x)^2$ at $y = 1$ and $v = 16a(t)y^2(1-y)^2$ at $x = 1$; (2) $u = 16a(t)x^2(1-x)^2$ at $y = 1$ and $v = -16a(t)y^2(1-y)^2$ at $x = 1$; (3) $u = 16a(t)x^2(1-x)^2$ at $y = 1$ and $u = -16a(t)x^2(1-x)^2$ at $y = 0$; and (4) $u = 16a(t)x^2(1-x)^2$ at $y = 1$ and $u = 16a(t)x^2(1-x)^2$ at $y = 0$. For all these cases, we have found that the moment-closure method produces very similar flow patterns as compared with the Monte Carlo results. Here, we just present the comparison of moment-closure and Monte Carlo simulations in terms of the flow and polymeric stress at $t = 50$ for the first boundary condition. The Monte Carlo result is an average of 3 independent simulation runs, each with 100 Brownian fields. Figure 5.4 shows the excellent agreement for the flow pattern, and one can also see that the overall profiles of the polymeric stress are in good agreement as well. Finally, it is interesting to notice that the moment-closure system strictly preserves the symmetry of the original coupled system of Navier–Stokes and Fokker–Planck equations, while the symmetry is lost (see the shear stress) in the Monte Carlo simulation due to the insufficient sampling of the normal distribution by a finite number of Gaussian random variables ΔW as used in (5.3).

Other physical parameters. The moment-closure method for other values of the physical parameters have also been tested. Roughly speaking, the polymer density λ determines the strength of the polymeric stress on the flow, the elasticity constant H affects the shape of the equilibrium dumbbell distribution, and the friction coefficient ζ defines a relaxation time and meanwhile places a weight on the influence of the flow on the dumbbell configuration. Due to the low resolution of our computational grid, the fluid viscosity ν is held to be a fixed value of $\nu = 10^{-3}$, and the moment-closure

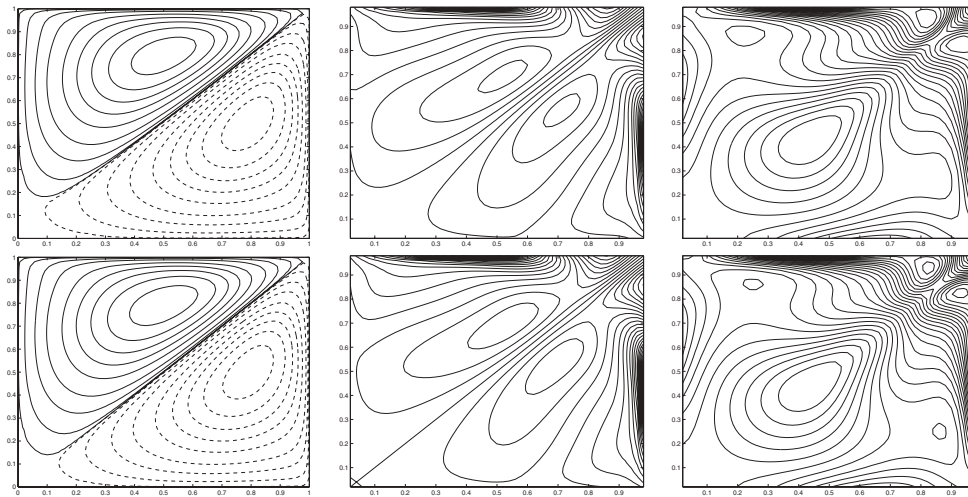


FIG. 5.4. Comparison of the stream function (left), normal stress (center), and shear stress (right) between Monte Carlo (top row) and moment-closure (bottom row) simulations for a different boundary condition. The horizontal velocity u at the top boundary and the vertical velocity v at the right boundary stabilize at $16x^2(1-x)^2$ and $16y^2(1-y)^2$, respectively.

method is examined as one of the parameters λ , H , and ζ is varied while others are kept fixed at the values used before for the driven-cavity problem.

In principle, we expect the moment-closure approximation to deteriorate as the flow field causes the dumbbell configuration to deviate more and more from its equilibrium PDF. Hence, we focus our attention on smaller values of H and bigger values of ζ , as a smaller H increases the vulnerability of the PDF to perturbation and a bigger ζ increases the effect of the flow field. On the other hand, since the weight λ determines how sensitive the flow field is to the error committed by the moment-closure approximation to the stress field, we will also be interested in examining the moment-closure method for larger values of λ . We now report our findings in words without overwhelming the readers with the supporting pictures. For λ as large as 0.1, or for H as small as 60, or for ζ as large as 80, we have found that the moment-closure method in all these cases gives flow fields in excellent agreement with the Monte Carlo results, which indicates that our moment-closure method is valid at least for a range of physical parameters.

However, as we further vary the parameters, the numerical solution to the moment-closure system becomes unstable. Taking λ as an example, we have found that the numerical solution becomes unstable for $\lambda = 0.15$. We have checked that refining the computational grid or time step does not recover the stability, and, more importantly, the corresponding Monte Carlo simulation becomes unstable as well for $\lambda = 0.15$ in a similar pattern. This indicates that the instability cannot be held as a weakness of the moment-closure approach. At this moment, it is perhaps premature to claim that the instability is an intrinsic feature of the original system (1.1)–(1.3). However, this may not be totally surprising, as the fluid viscosity is the only regularizing term of the system that may fail to control the nonsmoothness in the polymeric stress for large λ . In summary, for the test problem of driven-cavity flow in a square domain, we have found that the moment-closure approach gives satisfactory approximation in all cases that the numerical solution to the moment-closure system

can be obtained.

Finally, we make some comments about the limitation of the proposed closure approach. The most severe limitation of the model lies in that the approximation deteriorates as the shear or extension rates increase, as has been illustrated previously in the comparison of the closure prediction and the original FENE model in simple shear flow. This is due to our ansatz being based on perturbing the equilibrium PDF that cannot incorporate PDF shapes far from equilibrium.² This in fact points to a general problem of the closure approach relying on imposing a certain PDF ansatz. For example, the Bingham closure on liquid-crystalline polymers is shown to fail in predicting flow-aligning transition in simple shear due to its inability to produce skewing of the orientation distribution function [4]. On the other hand, it is not reasonable to request a reduced model via closure approximation to reproduce perfectly the behavior of the original kinetic theory at all ranges of physical parameters. So, the more practical criteria on closure models would be to see if they can produce good agreement with the original model for certain regimes of physical parameters, while the deviation from the original model at other regimes does not hinder their practical usage. In this perspective, we may indeed show that the proposed closure yields better quantitative agreement with the FENE model for weak flow than the FENE-P and FENE-L models, thanks to the explicit usage of the equilibrium PDF in the ansatz. We are currently investigating possibilities to augment the current model in order to reproduce at least qualitatively the behavior of FENE fluids for strong flow. One direction under consideration is to include systematically higher moment effects in the PDF ansatz. The results from this line of research will be reported elsewhere [8].

6. Conclusion. As opposed to the purely macroscopic approach, the advantage of the kinetic theory of polymeric fluids lies in its ability to provide detailed information on polymer structures. However, if one is mainly interested in macroscopic quantities such as flow field and stress distribution, it is desirable and sometimes necessary to derive effective macroscopic models from the exact microscopic description, leading to systems more amenable to analysis and computation. We have presented in this paper a moment-closure approach to derive macroscopic dynamics from the kinetic theory on FENE dumbbells. The closure approximation is based on a systematic procedure of restricting the probability distributions to a special class of smooth distribution functions. Such an approach may also be useful in more complex settings.

The simplified system for the FENE model considered here still possesses an energy law analogous to the original system. Mathematical analysis and numerical experiments have been carried out to ensure the well-posedness of the moment-closure system and to investigate the validity of the closure approximation. In particular, it is found that, in the simple shear flow case, the closure approach gives good agreement with the original Fokker–Planck equation for small shear rates. Good agreement between the original system and the moment-closure system is also found in simulating flows in a square domain with driven-cavity and other slip boundary conditions. In the simulations presented here, we have focused on steady-state flows in simple geometry. Further testings on the proposed model in terms of its time-dependent behavior and its effects on flows in complex geometry will be pursued in our future work.

²We would like to mention that although the idea of taking advantage of the equilibrium PDF in deriving closure relations has been extensively used in kinetic theory of gases, and also in deriving kinetic theory of macromolecular solutions [6], the assumption is usually made on the particle velocity distribution, and thus the approaches and difficulties are often quite different from ours.

Acknowledgment. We thank Prof. Weinan E and the referees for their valuable inputs on improving this work.

REFERENCES

- [1] R. B. BIRD, R. C. ARMSTRONG, AND O. HASSAGER, *Dynamics of Polymeric Fluids, Vol. 1, Fluid Mechanics*, John Wiley and Sons, New York, 1977.
- [2] R. B. BIRD, O. HASSAGER, R. C. ARMSTRONG, AND C. F. CURTISS, *Dynamics of Polymeric Fluids, Vol. 2, Kinetic Theory*, John Wiley and Sons, New York, 1977.
- [3] J. BONVIN AND M. PICASSO, *Variance reduction methods for CONNFESSIT-like simulations*, *J. Non-Newtonian Fluid Mechanics*, 84 (1999), pp. 191–215.
- [4] C. V. CHAUBAL AND L. G. LEAL, *A closure approximation for liquid-crystalline polymer models based on parametric density estimation*, *J. Rheology*, 42 (1998), pp. 177–201.
- [5] J.-Y. CHEMIN AND N. MASMOUDI, *About lifespan of regular solutions of equations related to viscoelastic fluids*, *SIAM J. Math. Anal.*, 33 (2001), pp. 84–112.
- [6] C. F. CURTISS, R. B. BIRD, AND O. HASSAGER, *Kinetic theory and rheology of macromolecular solutions*, *Advances in Chemical Physics*, 35 (1976), pp. 31–117.
- [7] M. DOI AND S. F. EDWARDS, *The Theory of Polymer Dynamics*, Clarendon Press, Oxford, UK, 1986.
- [8] Q. DU, C. LIU, AND P. YU, *FENE dumbbell model and its several linear and nonlinear closure approximations*, *Multiscale Model. Simul.*, submitted.
- [9] W. E AND J. LIU, *Vorticity boundary condition and related issues for finite difference schemes*, *J. Comput. Phys.*, 124 (1996), pp. 368–382.
- [10] W. E, T. LI, AND P. W. ZHANG, *Well-Posedness for the Dumbbell Model of Polymeric Fluids*, preprint, 2003.
- [11] J. FENG, C. V. CHAUBAL, AND L. G. LEAL, *Closure approximations for the Doi theory: Which to use in simulating complex flows of liquid-crystalline polymers*, *J. Rheology*, 42 (1998), pp. 1095–1119.
- [12] J. FENG AND L. G. LEAL, *Simulating complex flows of liquid-crystalline polymers using the Doi theory*, *J. Rheology*, 41 (1997), pp. 1317–1335.
- [13] G. FOREST, Q. WANG, AND R. ZHOU, *Full-tensor alignment criteria for sheared nematic polymers*, *J. Rheology*, 47 (2003), pp. 105–127.
- [14] M. GROSSO, P. L. MAFFETTONE, AND F. DUPRET, *A closure approximation for nematic liquid crystals based on the canonical distribution subspace theory*, *Rheol. Acta*, 39 (2000), pp. 301–310.
- [15] M. GROSSO, P. L. MAFFETTONE, P. HALIN, R. KEUNINGS, AND V. LEGAT, *Flow of nematic polymers in eccentric cylinder geometry: Influence of closure approximations*, *J. Non-Newtonian Fluid Mechanics*, 94 (2000), pp. 119–134.
- [16] E. J. HINCH AND L. G. LEAL, *Constitutive equations in suspension mechanics. Part 2. Approximate forms for a suspension of rigid particles affected by Brownian rotations*, *J. Fluid Mech.*, 76 (1976), pp. 187–208.
- [17] M. HULSEN, A. VAN HEEL, AND B. VAN DEN BRULE, *Simulation of viscoelastic flows using Brownian configuration fields*, *J. Non-Newtonian Fluid Mechanics*, 70 (1997), pp. 79–101.
- [18] B. JOURDAIN, T. LELIEVRE, AND C. LE BRIS, *On a variance reduction technique for the micro-macro simulations of polymeric fluids*, *J. Non-Newtonian Fluid Mechanics*, to appear.
- [19] B. JOURDAIN, T. LELIEVRE, AND C. LE BRIS, *Existence of solution for a micro-macro model of polymeric fluid: The FENE model*, *J. Funct. Anal.*, to appear.
- [20] B. JOURDAIN, T. LELIEVRE, AND C. LE BRIS, *Numerical analysis of micro-macro simulations of polymeric fluid flows: A simple case*, *Math. Models Methods Appl. Sci.*, 12 (2002), pp. 1205–1243.
- [21] O. A. LADYZHENSKAYA, *The Mathematical Theory of Viscous Incompressible Flow*, Gordon and Breach, New York, 1969.
- [22] M. LASO AND H. C. OTTINGER, *Calculation of viscoelastic flow using molecular models: The CONNFESSIT approach*, *J. Non-Newtonian Fluid Mechanics*, 47 (1993), pp. 1–20.
- [23] G. LIELENS, P. HALIN, I. JAUMAIN, R. KEUNINGS, AND V. LEGAT, *New closure approximations for the kinetic theory of finitely extensible dumbbells*, *J. Non-Newtonian Fluid Mechanics*, 76 (1998), pp. 249–279.
- [24] G. LIELENS, R. KEUNINGS, AND V. LEGAT, *The FENE-L and FENE-LS closure approximations to the kinetic theory of finitely extensible dumbbells*, *J. Non-Newtonian Fluid Mechanics*, 87 (1999), pp. 179–196.
- [25] A. LOZINSKI AND C. CHAUVIERE, *A fast solver for Fokker-Planck equation applied to viscoelastic flows calculations: 2D FENE model*, *J. Comput. Phys.*, 189 (2003), pp. 607–625.

- [26] H. C. OTTINGER, *Stochastic Processes in Polymeric Fluids, Tools and Examples for Developing Simulation Algorithms*, Springer-Verlag, Berlin, 1996.
- [27] H. C. OTTINGER, B. VAN DEN BRULE, AND M. A. HULSEN, *Brownian configuration fields and variance reduced CONNFESSIT*, *J. Non-Newtonian Fluid Mechanics*, 70 (1997), pp. 255–261.
- [28] R. OWENS AND T. PHILLIPS, *Computational Rheology*, Imperial College Press, London, 2002.
- [29] N. PHAN-THIEN AND R. I. TANNER, *A new constitutive equation derived from network theory*, *J. Non-Newtonian Fluid Mechanics*, 2 (1977), pp. 353–365.
- [30] R. TEMAM, *Navier-Stokes Equations, Theory and Numerical Analysis*, North-Holland, Amsterdam, 1984.
- [31] Q. WANG, *Comparative studies on closure approximations in flows of liquid crystal polymers: I. Elongational flows*, *J. Non-Newtonian Fluid Mechanics*, 72 (1997), pp. 141–162.
- [32] Q. WANG, *Comparative studies on closure approximations in flows of liquid crystal polymers: II. Fiber flows*, *J. Non-Newtonian Fluid Mechanics*, 72 (1997), pp. 163–185.